JOURNAL OF CATALYSIS **175,** 236–244 (1998)
ARTICLE NO. CA981998

Ethanol Synthesis from Carbon Dioxide on $[Rh_{10}Se]/TiO_2$ Catalyst Characterized by X-Ray Absorption Fine Structure Spectroscopy

Yasuo Izumi,[1] Hiroshi Kurakata, and Ken-ichi Aika

Department of Environmental Chemistry and Engineering, Interdisciplinary Graduate School of Science and Engineering, Tokyo Institute of Technology, 4259 Nagatsuta, Midori-ku, Yokohama 226, Japan

Received August 21, 1997; revised November 26, 1997; accepted November 29, 1997

The active site structures and electronic states were studied for the $[Rh_{10}Se]/TiO_2$ catalyst by means of edge spectra and EXAFS. The rate and selectivity of ethanol synthesis from CO_2 on $[Rh_{10}Se]/TiO_2$ had strong dependence on the heating temperature in vacuum (T_{evac}) (1). Corresponding to the maximum of rate and selectivity when the T_{evac} was 623 K, the distance r_{Se-Rh} reached a minimum (2.41 Å) by Se K- and Rh K-edge EXAFS analyses. The contracted $[Rh_{10}Se]$ cluster was found to have an electronic state similar to that of Rh_3Se_8 or $RhSe_2$ rather than of metallic Rh. A new reaction path control is proposed by regulating the distance between the interstitial Se atom and the metal framework $[Rh_{10}]$. A strong peak due to $1s \rightarrow np$ transition was observed around the Se K absorption edge. The peak intensity did not exhibit significant change when the T_{evac} was varied for $[Rh_{10}Se]/TiO_2$. On the other hand, the area of peak observed around 23,230 eV in Rh K-edge spectra gradually decreased when the T_{evac} was elevated for $[Rh_{10}Se]/TiO_2$. Hence, the Se atom surrounded by $[Rh_{10}]$ framework was always kept in anionic state, while the electronic state of Rh atoms gradually changed by the interaction with TiO_2 surface. The change for Rh atoms was also supported by the gradual increase of r_{Rh-Rh} obtained by EXAFS with the temperature increase. In the case of Rh sites with lower total coordination number around Rh ($[Rh_{10}Se]/SiO_2$, $[Rh_{10}Se]/Al_2O_3$, and $[Rh_{10}Se]/MgO$), the reaction $CO_2 \rightarrow CO(a) + O(a)$ occurred predominantly and formed CO(a) poisoned the catalysis.

INTRODUCTION

The increased emission of carbon dioxide is one of the major environmental problems. It is desirable to convert CO_2 into useful chemicals effectively. New catalyst $[Rh_{10}Se]/TiO_2$ was reported which synthesized ethanol from $CO_2 + H_2$ (1). The activity was high ($\approx$8.0 mol · cluster^{-1} min^{-1}) and the conversion reached to 80% within 15 min (47 kPa of reaction gas; 0.3 g of catalyst) compared to the other supported Rh catalysts. The selectivity was also very good ($\approx$83%). Promoting effect of Se was implied similar to reported bimetallic catalysts (2, 3).

Detailed characterizations were difficult because (more than) two elements coexist in bimetallic catalysts. XAFS (X-ray absorption fine structure) spectroscopy is one of the best tools to study bimetallic catalysts owing to the tunability of absorption edge of elements (3). Lee *et al.* (4) reported the selective benzene synthesis from acetylene on Au/Pd colloid catalyst. The synthesis rate increased as the heating temperature of the colloid was elevated. According to the temperature increase, Pd skin formation around Au core was suggested by EXAFS and also the decrease of Pd 4d vacancy was suggested by monitoring the $1s \rightarrow 4d$ transition around Pd K-edge. The $[Rh_{10}Se]$ cluster consisted of eleven atoms has an advantage to escape from the statistical uncertainty which bimetallic particles of larger size (20–100 Å) have in XAFS analysis (4–6). A wide variety of metal clusters was supported on inorganic oxides, where the metal framework was stabilized through the metal-$O_{(s)}$ ($O_{(s)}$: oxygen atom at surface) bondings (7). The promoting effects of anionic Se were reported by modifying the electronic state of active site of Rh/MgO, Rh/ZrO_2, or Rh/SiO_2 or by the direct coordination of Se to surface intermediate species in ethene hydroformylation (8–10). Simple promoting mechanism is expected when the Se is incorporated inside the metal cluster framework $[Rh_{10}]$.

In this paper, the origin of ethanol synthesis from CO_2 is discussed in terms of the effects of Se by means of XAFS spectroscopy. The active site structures of $[Rh_{10}Se]$ on TiO_2 for ethanol synthesis were characterized by Rh K-edge and Se K-edge EXAFS. The change of distance between interstitial Se and framework $[Rh_{10}]$ was monitored when the catalyst preparation conditions were varied. The strength of the interaction between Se and $[Rh_{10}]$ can be monitored by the distance r_{Se-Rh} besides the each Rh K-edge and Se K-edge structure changes. On the basis of electronic state and the cluster structure, the reaction mechanism of ethanol synthesis is proposed.

[1] Correspondence should be addressed. E-mail: yizumi@chemenv.titech.ac.jp.

0021-9517/98 $25.00

EXPERIMENTAL

Sample Preparation and Catalysis

The supported cluster was prepared from $[PPN]_2[Rh_{10}Se(CO)_{22}]$ (**1**) crystal (PPN = N(PPh$_3$)$_2$) (Fig. 1). The cluster was synthesized from $Rh_4(CO)_{12}$ and [PPN][SeCN] (11, 12). The TiO_2(P25), Al_2O_3(alon C), and SiO_2(Davison 952) were treated at 573 K under vacuum for 2 h prior to use as supports. MgO was prepared from $Mg(OH)_2$ by heating at 773 K for 2 h in vacuum. The (**1**) was reacted with each oxide at 290 K for 2 h in purified THF in Ar atmosphere, with subsequent removal of THF in vacuum. In order to obtain enough large edge jump (>0.25) at Se K-edge and Rh K-edge (transmission mode), the loadings of Rh were fixed to 1.3 (TiO_2 and Al_2O_3), 2.8 (SiO_2), and 1.6 wt% (MgO) in consideration of the BET surface area (50 for TiO_2, 100 for Al_2O_3, 300 for SiO_2, and 200 $m^2\ g^{-1}$ for MgO). Thus-prepared catalysts are denoted $[Rh_{10}Se]$/oxide. The incipient cluster catalysts were totally decarbonylated by heating in vacuum at 593–813 K, followed by the treatment in H_2 at 623 K. When the catalysts were heated in vacuum at 523 K, they were treated in H_2 at 523 K.

Conventional Rh/TiO_2 catalyst was impregnated from water solution of $Rh(NO_3)_3$. After the evaporation of water, the powder was treated in O_2(1 h) and then in H_2(1 h) at 523 K. The loading of Rh was 0.5 wt%. Rh_3Se_8 powder was synthesized from elemental Rh and Se in the reported procedure (13). The reaction was carried out under 47 kPa of $CO_2 + H_2$ ($CO_2 : H_2 = 1 : 2$) in the temperature range 523–623 K in a closed circulation system (dead volume 210 cm^3). The products were analyzed by gas chromatography and mass spectroscopy (1).

XAFS Measurements

The Rh K-edge and Se K-edge XAFS spectra were measured at room temperature at the beamlines 10B and 6B of the Photon Factory in the National Laboratory for High Energy Physics (KEK-PF) (Proposal No. 95G226). The accumulation ring energy was 2.5 GeV and the ring current was 360–290 mA. All the spectra were measured at 10B except for Se K-edge of $[Rh_{10}Se]/TiO_2$ (beamline 6B). The beamline 10B utilized the channel-cut double crystal monochrometer of Si(311). The incident and transmitted X-ray were monitored by ion chambers filled with Ar for I_0 and Kr for I. The beamline 6B utilized double crystal monochrometer of Si(111). The beam was focused by the sagittal focus of second crystal. The incident and fluorescence X-ray were monitored by ion chambers filled with the mixture of $Ar(15\%) + N_2(85\%)$ for I_0 and Ar for I. A 30 μm-filter of As (K-edge $\approx$ 11,875 eV) was located between the sample and the ion chamber for I. The XAFS spectrum for Se powder was measured also at 6B in the same conditions as for $[Rh_{10}Se]/TiO_2$ as comparison.

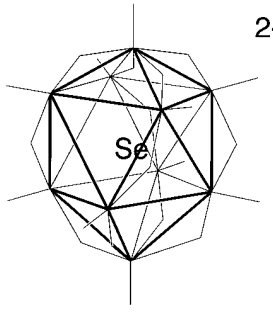

FIG. 1. The structure of $[Rh_{10}Se(CO)_{22}]^{2-}$ inferred from the structure of $[Rh_{10}S(CO)_{22}]^{2-}$ determined by X-ray crystallography (12). Carbonyl ligands are not shown for clarity.

Edge Spectra Analysis

The photon energy was calibrated by equalizing the derivative maximum of the absorption edge of Se powder 12,654.5 eV for Se K-edge and that of Rh foil 23,219.8 eV for Rh K-edge. The background was subtracted by fitting the polynomial to the preedge region and extrapolating it to postedge region. The edge jump of subtracted spectrum was normalized at 12,670.0 eV (Se K-edge) or 23,270.0 eV (Rh K-edge).

A strong peak was observed around Se K absorption edge. In order to evaluate the peak area, the normalized edge spectra were analyzed by non-linear least square curve fitting (14). The arctangent function was used as the absorption edge. The mixture of Gaussian (G) and Lorentzian (L) was used as the strong peak around the edge. Generally, the Gaussian line width represents the energy resolution of apparatus (14, 15). On the basis of the preliminary curve fitting for more than ten spectra, the FWHM (full width at half maximum) of G was fixed: 3.6 and 4.9 eV for spectra measured at 10B and 6B, respectively. The Lorentzian line width represents the natural line width, which was fixed to 2.1 eV (16). The intensity ratio of G : L was fixed to 1 : 1. The broader feature in the range 12,662–12,680 eV was easily reproduced by two L functions. The peak deconvolution in the range 12,650–12,680 eV was performed with these five functions (arctangent, G + L, and two L). Alternative peak deconvolution in the region 12,650–12,660 eV was also performed with the arctangent function and the mixture of G and L functions (three functions).

EXAFS Analysis

The EXAFS spectra were analyzed by the program EXAFSH (17). The background subtraction was performed by calculating the three-block cubic spline, followed by normalization by using the Victoreen parameter. The Fourier transform of k^3-weighted χ function was carried out over the range $k_{min} = 3$ and $k_{max} = 12.5$–15.0 $Å^{-1}$. The filtered inverse Fourier transform was performed in the

range $r_{min} = 1.50–1.60$ and $r_{max} = 2.65–2.75$ Å for Se K-edge EXAFS and $r_{min} = 1.30–1.60$ and $r_{max} = 2.75–2.90$ Å for Rh K-edge EXAFS.

The curve fitting analysis was performed in the range $k_{min} = 4$ and $k_{max} = 12–14$ Å^{-1} by utilizing the empirical phase shift and amplitude functions extracted from the EXAFS of model compounds: Rh foil for Rh–Rh bond (2.689 Å), Rh_3Se_8 powder for Rh–Se bond (2.498 Å) (13), Rh_2O_3 powder for Rh–O bond (2.05 Å) (18), [PPN] $[Rh_3Se_2(CO)_6]$ (**2**) crystal for Se–Rh bond (2.458 Å) (11), and SeO_2 powder for Se–O bond (1.76 Å) (19). The goodness of the fit was estimated by the R factor.

$$R_f = \int |k^3\chi_{obs} - k^3\chi_{calc}|^2 \, dk \Big/ \int |k^3\chi_{obs}|^2 \, dk.$$

RESULTS

Ethanol Synthesis from CO_2 on $[Rh_{10}Se]/TiO_2$

The ethanol synthesis rates, turnover numbers per surface Rh, and ethanol selectivities are summarized in Table 1 in relation to the effects of Se and support on the ethanol synthesis. Ethanol synthesis was observed only on $[Rh_{10}Se]/TiO_2$. The $[Rh_{10}Se]$ clusters on the other supports had very poor (*or* no) activities; the $[Rh_{10}Se]/Al_2O_3$ and $[Rh_{10}Se]$/MgO produced methane and/or CO, and the $[Rh_{10}Se]/SiO_2$ had entirely no activity. The conventional Rh/TiO_2 had the intermediate activity compared to supported $[Rh_{10}Se]$ catalysts, but did not produce ethanol.

The initial rate and selectivity of ethanol synthesis exhibited strong dependence on the heating temperature (523–813 K) in vacuum (T_{evac}) (Table 1). Both the initial rate and selectivity were best when the T_{evac} was 623 K. The production rate of CH_4 and/or CO did not show significant change when the T_{evac} was varied.

Se Absorption Spectra

The Se K-edge spectra are shown in Fig. 2A for supported $[Rh_{10}Se]$ clusters and reference compounds. A strong peak was observed around absorption edge in all the spectra. The peak intensity was relatively weak for (**1**) (b) and $[Rh_{10}Se]/TiO_2$ (e). Only the spectra of Se powder (c, d) did not have an evident feature within the range of 12663–8 eV, different from the others.

The dependence on the T_{evac} was examined for $[Rh_{10}Se]/TiO_2$ (Fig. 2B). The shape was very similar to each other for the three (i–k). The edge position shifted by heating: by $+0.2$ eV from 523 to 623 K and by -0.6 eV from 623 to 813 K. As a result, the edge energy had the maximum when the sample was heated at 623 K.

As the peak is very near the edge, the area was evaluated by peak deconvolution (Fig. 2C). When the curve fitting was tried with arctangent (as edge) and G + L (as strong peak around edge) in the range 12,650–12,660 eV, it was difficult to determine the height of arctangent. Besides, the fitting was not good when the FWHM for G was fixed (the unfixed FWHM varied in the range 3.4–4.7 for spectra obtained at beamline 10B). Therefore, the least square fitting calculation was performed with five functions: arctangent, G + L, and two L functions in the range 12,650–12,680 eV. The results are listed in Table 2. The normalized peak area exhibited almost no change (4.2–4.3) for the $[Rh_{10}Se]/TiO_2$ heated at 523–813 K. The normalized peak area was in the following order $[Rh_{10}Se]/TiO_2 <$ (**1**) $< [Rh_{10}Se]/MgO < [Rh_{10}Se]/SiO_2 \approx [Rh_{10}Se]/Al_2O_3 < Se \approx Rh_3Se_8$. The normalized peak area for the Se powder had a difference of 23% when the spectra were observed at different beamline. The above order of peak area should be discussed taking the difference of beamline into account. The difference was mainly due to the difference of monochrometer face used.

Rh Absorption Spectra

The Rh K-edge spectra was observed for supported $[Rh_{10}Se]$ catalysts and (**1**) (Fig. 3). The edge positions for $[Rh_{10}Se]/TiO_2$, $[Rh_{10}Se]/SiO_2$, $[Rh_{10}Se]/Al_2O_3$, and $[Rh_{10}Se]$/MgO fell within the range 23,211.9–23,212.4 eV when the sample was heated at 623–653 K in vacuum. When the T_{evac} was varied (523, 623, and 813 K) for $[Rh_{10}Se]/TiO_2$,

TABLE 1

The CO_2–H_2 Reactions on Supported $[Rh_{10}Se]$ Catalysts and Conventional Rh/TiO_2

Catalyst	Rh wt%	T_{evac}/K	T_{react}/K	Initial rate/10^{-3} mol h^{-1} g$_{cat}^{-1}$		TOF/min^{-1} [a]		Ethanol selectivity/mol%
				Ethanol	Methane + CO	Ethanol	Methane + CO	
$[Rh_{10}Se]/TiO_2$	1.3	523	523	0.09	0.6	0.012	0.079	13
		623	523	1.9	0.4	0.25	0.053	83
		813	523	0.9	0.4	0.12	0.053	71
$[Rh_{10}Se]/Al_2O_3$	1.3	653	623	0	0.2	0	0.026	0
$[Rh_{10}Se]$/MgO	1.6	623	623	0	0.04	0	0.004	0
$[Rh_{10}Se]/SiO_2$	2.8	623	623	0	0	0	0	0
Rh/TiO_2	0.5	523	623	0	1.8	0	(0.62)	0

Note. Total pressure 47 kPa. $P_{CO_2} : P_{H_2} = 1 : 2$.

[a] Turnover per surface Rh assuming 100% exposure of Rh to catalyst surface.

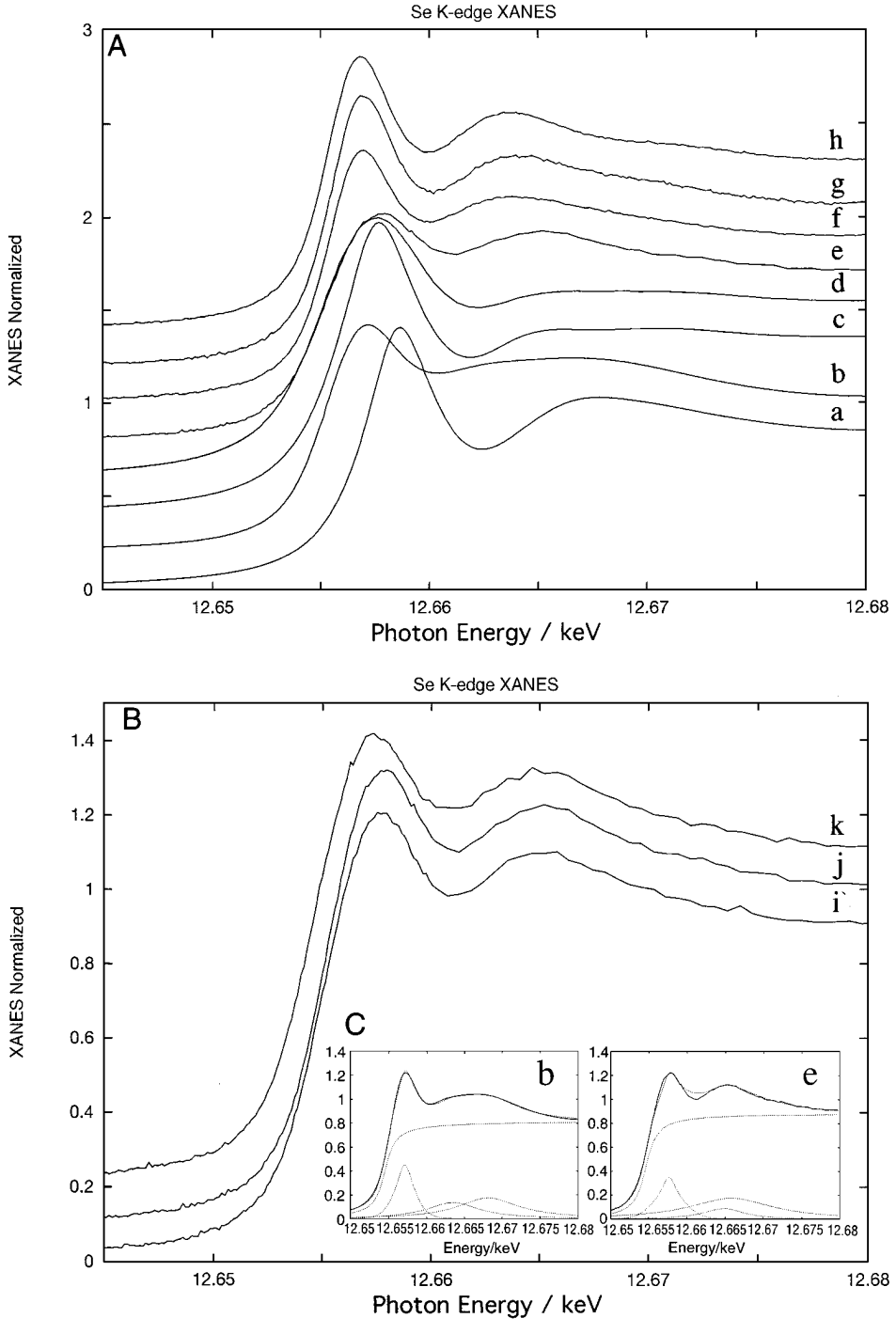

FIG. 2. Se K-edge spectra. (**A**) Rh_3Se_8 powder (a), crystal (**1**) (b), Se powder at beamline 10B (c), and at 6B (d), $[Rh_{10}Se]/TiO_2$ (e), $[Rh_{10}Se]/MgO$ (f), $[Rh_{10}Se]/Al_2O_3$ (g), and $[Rh_{10}Se]/SiO_2$ (h). (e)–(h), heated in vacuum at 623–653 K. (**B**) $[Rh_{10}Se]/TiO_2$ heated in vacuum at 523 (i), 623 (j), and 813 K (k). (**C**) Peak deconvolution analysis for crystal (**1**) and $[Rh_{10}Se]/TiO_2$ (623 K).

the edge positions were 23,214.1, 23,211.9, and 23,212.3 eV, respectively. It reached a minimum when the T_{evac} was 623 K.

The peak **A** in Fig. 3 gradually decreased as the T_{evac} was elevated for $[Rh_{10}Se]/TiO_2$ (a–d). The change looks small, but evident when the derivative spectra are plotted (not shown). The intensities of peak **A** for $[Rh_{10}Se]/SiO_2$ (e), $[Rh_{10}Se]/Al_2O_3$ (f), and $[Rh_{10}Se]/MgO$ (g) were similar to those for $[Rh_{10}Se]/TiO_2$ of $T_{evac} = 813$ K (d), 623 K (c), and 523 K (b), respectively.

TABLE 2

The Positions (E/eV = 12650 + α) of Se K Absorption Edge and First Peak Area

Sample	T_{evac}/K	Edge α/eV[a]	First peak area[b]
$[Rh_{10}Se]/TiO_2$	523	4.4	4.3
	623	4.6	4.2
	813	4.0	4.3
$[Rh_{10}Se]/SiO_2$	623	5.0	6.9
$[Rh_{10}Se]/Al_2O_3$	653	5.1	6.9
$[Rh_{10}Se]/MgO$	623	5.0	5.7
$[Rh_{10}Se(CO)_{22}]^{2-}$		4.5	4.9
Rh_3Se_8		6.1	8.0
Se powder		4.5	8.4

[a] The maximum point of derivative for arctangent function.
[b] The peak area of the mixture function normalized by the height of arctangent function.

Se EXAFS

In the k^3-weighted Fourier transform of χ function, a strong peak was observed around 2.1 Å (phase shift uncorrected) for $[Rh_{10}Se]/TiO_2$ of $T_{evac} = 623$ K (Fig. 4c). The Se K edge jump coincided with the calculated value from the impregnated amount of crystal (**1**) on TiO_2, and the edge jump did not change when the heating temperature was elevated up to 813 K. Hence, Se atom remained in catalyst in the whole procedure, and one-wave fitting of Se–Rh was tested. The result was $r_{Se-Rh} = 2.41$ Å and coordination number N_{Se-Rh} was 8.2 ($R_f = 4.9\%$). The fitting was not satisfactory, especially in lower wave number region. A close inspection of Fig. 4c indicates a shoulder on the lower-distance side than the main Se–Rh peak. Therefore, two-wave fitting was tried with Se–Rh and Se–O as a possibility that the bonding of Se with the $O_{(s)}$ of TiO_2 was formed. The best fit results were summarized in Table 3. The R_f was improved to 3.0%. The obtained $r_{Se-O_{(s)}}$ (1.97 Å) did not contradict with attached $[Rh_{10}Se]$ structure model on TiO_2 with the obtained distances r_{Se-Rh}, r_{Rh-Rh}, and $r_{Rh-O_{(s)}}$, and their coordination numbers (Fig. 5, discussed later).

In a similar procedure, curve fitting results were obtained for $[Rh_{10}Se]/TiO_2$ of $T_{evac} = 813$ K ($r_{Se-Rh} = 2.42$ Å and $r_{Se-O_{(s)}} = 1.98$ Å) and $[Rh_{10}Se]/SiO_2$ ($r_{Se-Rh} = 2.42$ Å and $r_{Se-O_{(s)}} = 1.95$ Å). As the EXAFS for $[Rh_{10}Se]/TiO_2$ of $T_{evac} = 523$ K was not fit with the two waves, the result of one-wave fitting was listed in Table 3. In summary, when the T_{evac} was varied for $[Rh_{10}Se]/TiO_2$, the r_{Se-Rh} value reached the minimum (2.41 Å) at 623 K. The Se–O bonding appeared when the T_{evac} was higher than 623 K.

Rh EXAFS

The temperature-programmed gas desorption was monitored for incipient supported $[Rh_{10}Se]$ clusters. Because almost all the gas desorption ($CO + CO_2$) occurred below 523–573 K originating from the carbonyl ligands of (**1**), curve fitting analysis was performed with two waves

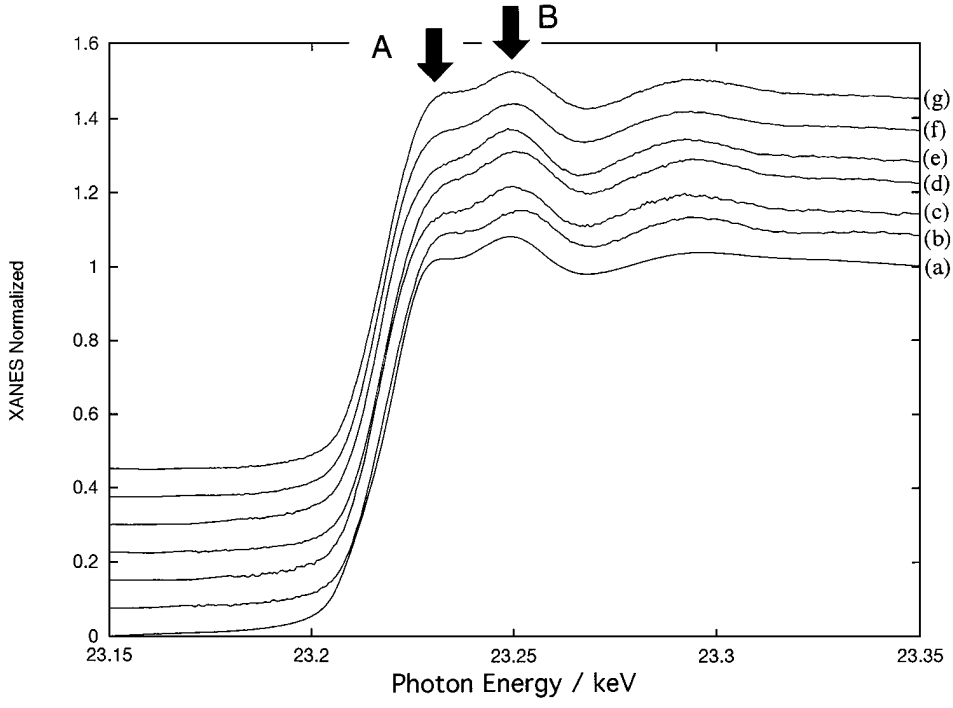

FIG. 3. Rh K-edge spectra. Crystal (**1**) (a), $[Rh_{10}Se]/TiO_2$ heated in vacuum at 523 (b), 623 (c), and 813 K (d), $[Rh_{10}Se]/SiO_2$ (e), $[Rh_{10}Se]/Al_2O_3$ (f), and $[Rh_{10}Se]/MgO$ (g).

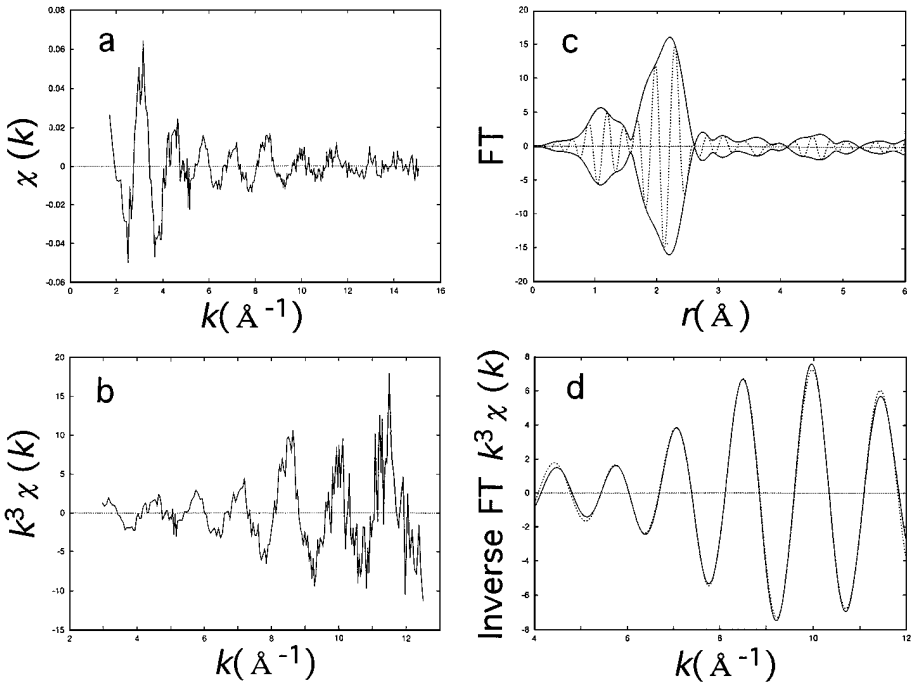

FIG. 4. Se K-edge EXAFS for $[Rh_{10}Se]/TiO_2$ heated in vacuum at 623 K: (a) χ function; (b) k^3-weighted χ function; (c) its associated Fourier transform; and (d) inversely Fourier-transformed $k^3\chi(k)$ function and curve fitting.

(Rh–Rh and Rh–Se) or three waves (Rh–Rh, Rh–Se, and Rh–$O_{(s)}$). As the N_{Se-Rh} obtained from Se K-edge EXAFS did not significantly change from ten for crystal (**1**) considering the errors (Table 3), the N_{Rh-Se} was fixed at 1.0 in Rh K-edge curve fitting procedure. In all the cases of supported $[Rh_{10}Se]$ clusters, the R_f was always significantly better with three waves than with two waves. The obtained $r_{Rh-O_{(s)}}$ and $N_{Rh-O_{(s)}}$ did not contradict attached $[Rh_{10}Se]$ structure model on TiO_2 with the obtained distances r_{Se-Rh} and r_{Rh-Rh}, and their coordination numbers (Fig. 5, discussed later).

The best fit results are summarized in Table 4. The N_{Rh-Rh} was 4.8 for $[Rh_{10}Se]/TiO_2$ of $T_{evac} = 523$ K. The anion of (**1**) has average N_{Rh-Rh} of 4.8 (Fig. 1). According to the increase of heating temperature, the r_{Rh-Rh} and $N_{Rh-O_{(s)}}$ values gradually increased, while the N_{Rh-Rh} value gradually decreased. The obtained r_{Rh-Se} values coincided with corresponding r_{Se-Rh} values (Table 3) within the error of 0.01 Å. It should be noted that the total coordination number around Rh atom ($= N_{Rh-Rh} + N_{Rh-Se} + N_{Rh-O_{(s)}}$) was classified into two ranges: 6.4 ± 0.7 for $[Rh_{10}Se]/TiO_2$ and 5.5 ± 0.2 for $[Rh_{10}Se]/SiO_2$, $[Rh_{10}Se]/Al_2O_3$, and $[Rh_{10}Se]$/MgO.

DISCUSSION

The ethanol synthesis from CO_2 was observed exclusively on $[Rh_{10}Se]/TiO_2$ (Table 1). The synthesis rate was best when the evacuation temperature was 623 K. The total

TABLE 3

The Results of Curve Fitting Analysis of Se K-Edge EXAFS for $[Rh_{10}Se]/TiO_2$ and $[Rh_{10}Se]/SiO_2$

		Se–Rh[a]			Se–O[b]			
Sample	T_{evac}/K	N	r/Å	$\Delta(\sigma^2)/10^{-3}$ Å^2	N[c]	r/Å	$\Delta(\sigma^2)/10^{-3}$ Å^2	R_f/%
$[Rh_{10}Se]/TiO_2$	523	10	2.44	3.8	—	—	—	3.1[d]
	623	8.6	2.41	4.5	(1.0)	1.97	−1.6	3.0
		(±1.2)	(±0.007)			(±0.019)		
	813	9.5	2.42	3.3	(1.0)	1.98	−1.4	0.6
$[Rh_{10}Se]/SiO_2$	623	9.1	2.42	4.6	(1.0)	1.95	−0.3	1.3

[a, b] Empirical model parameters extracted from crystal (**2**)[a] and SeO_2 powder[b]. Debye–Waller factors are relative values compared to these references.
[c] Fixed value.
[d] Not fitted with two waves.

TABLE 4

The Results of Curve Fitting Analysis of Rh K-Edge EXAFS for Supported [$Rh_{10}Se$] Clusters

Sample	T_{evac}/K	Rh–Rh[a] N	Rh–Rh[a] r/Å	Rh–Rh[a] $\Delta(\sigma^2)/10^{-3}$ Å^2	Rh–Se[b] N[d]	Rh–Se[b] r/Å	Rh–Se[b] $\Delta(\sigma^2)/10^{-3}$ Å^2	Rh–O[c] N	Rh–O[c] r/Å	Rh–O[c] $\Delta(\sigma^2)/10^{-3}$ Å^2	R_f/%
[$Rh_{10}Se$]/TiO_2	523	4.8	2.69	5.3	(1.0)	2.45	4.4	1.2	2.10	1.3	0.10
	623	4.0	2.72	6.0	(1.0)	2.41	1.6	1.5	2.09	1.9	0.12
		(±0.6)	(±0.001)			(±0.012)		(±0.6)	(±0.008)		
	813	3.0	2.75	2.0	(1.0)	2.43	−0.7	1.7	2.13	6.9	0.41
[$Rh_{10}Se$]/SiO_2	623	2.9	2.74	3.0	(1.0)	2.42	1.3	1.4	2.13	1.5	0.17
[$Rh_{10}Se$]/Al_2O_3	653	3.7	2.72	5.5	(1.0)	2.41	0.8	0.9	2.05	−0.7	0.33
[$Rh_{10}Se$]/MgO	623	2.7	2.70	5.7	(1.0)	2.39	2.1	2.0	2.18	5.0	0.69

[a, b, c] Empirical model parameters extracted from Rh foil,[a] Rh_3Se_8,[b] and Rh_2O_3.[c] Debye–Waller factors are relative values compared to these references.

[d] Fixed value.

conversion rate was in the order [$Rh_{10}Se$]/TiO_2 > conventional Rh/TiO_2 > [$Rh_{10}Se$]/Al_2O_3 > [$Rh_{10}Se$]/MgO > [$Rh_{10}Se$]/SiO_2. The [$Rh_{10}Se$]/TiO_2 had remarkable dependence on the T_{evac} in terms of rate and selectivity.

The [$Rh_{10}Se$] Structure on Oxides and Its Transformation

The curve fitting results of Rh K-edge EXAFS were summarized in Table 4. With regard to [$Rh_{10}Se$]/TiO_2, the coordination number of Rh–Rh bond was 4.8 when heated at 523 K. It is the same value as (**1**). Hence, the totally-decarbonylated (**1**) by the evacuation at 523 K was attached on TiO_2 without significant structure change of the [$Rh_{10}Se$] framework (Fig. 1). One of the [Rh_3] faces of polyhedral [$Rh_{10}Se$] may interact with $O_{(s)}$ atoms (Fig. 5a). The unchanging edge jump of Se K-edge for all the samples when the crystal was impregnated on oxides also supported the retention of stable [$Rh_{10}Se$] unit. By heating to 623 K, the N_{Rh-Rh} decreased to 4.0, while the $N_{Rh-O_{(s)}}$ increased to 1.5. One of the explanations for the change is that the Rh–Rh bonds around the [Rh_3] triangle face were cleaved by the additional formation of Rh–$O_{(s)}$ bondings at 623 K (Fig. 5b). By further heating to 813 K, the N_{Rh-Rh} further decreased (3.0) and the $N_{Rh-O_{(s)}}$ further increased (1.7). The treatment in H_2 (523–623 K) had negligible effect on the EXAFS results in Tables 3 and 4.

The aggregation of metal clusters is plausible on support in these or more severe conditions (7). The fragmentation of [$Rh_{10}Se$] into smaller portions is unlikely based on the unchanging N_{Se-Rh} values (≈10, Table 3). The gradual decrease of N_{Rh-Rh} according to the increase of temperature contradicts the aggregation of [$Rh_{10}Se$] (Table 4), supporting the unimodal [$Rh_{10}Se$] cluster model given in Fig. 5, owing to the stabilization effect of [Rh_{10}] framework by Se. Although EXAFS has a weak point to measure the average of bulk, the majority of clusters in this case should remain integral and increase the interaction with TiO_2 as the temperature increases.

The r_{Rh-Se} value obtained from Rh K-edge EXAFS reached a minimum (2.41 Å) when the T_{evac} was 623 K. The

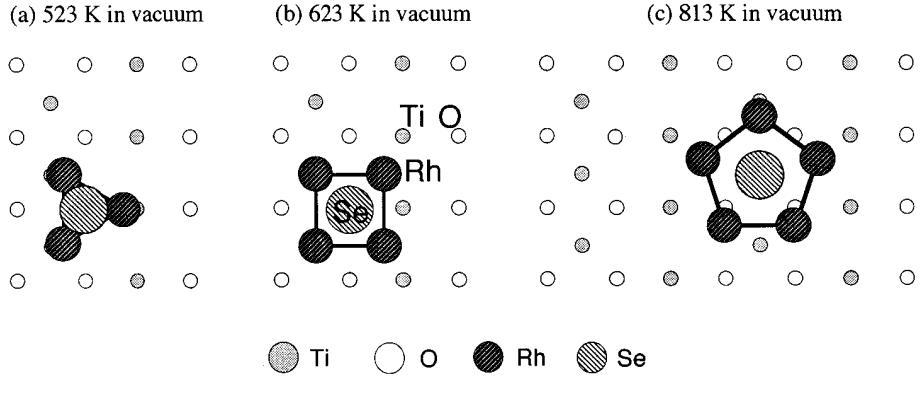

FIG. 5. Proposed model structures of [$Rh_{10}Se$] on TiO_2(110) surface. Heated in vacuum at 523 (a), 623 (b), and 813 K (c). Only the interface part of [$Rh_{10}Se$] framework is drawn for clarity.

r_{Se-Rh} values obtained from Se K-edge EXAFS (Table 3) coincided with the r_{Rh-Se} values within the error of 0.01 Å. The EXAFS analysis was very reliable by the curve fitting analysis from both edges.

The dependence of ethanol synthesis rate on the T_{evac} for $[Rh_{10}Se]/TiO_2$ is explained by the EXAFS results as follows. The key should be the change of r_{Rh-Se}. The synthesis rate had the maximum and the r_{Rh-Se} value reached the minimum when the T_{evac} was 623 K. The minimum r_{Rh-Se} was shorter by 0.02–0.09 Å than the r_{Rh-Se} of Rh_3Se_8 alloy (2.498 Å) (13), crystal (**2**) (2.458 Å) (11), or chemical-vapor-deposited Se on $[Rh_6]/MgO$ (2.43–2.44 Å) (10). On the basis of the shortest distance of Se–Rh, the electronic state of $[Rh_{10}Se]$ should become similar to Rh selenide (Rh_3Se_8 or $RhSe_2$). It was reported that the cationic transition metal catalyzed the CO associative reactions rather than the CO dissociative reactions (20).

As the T_{evac} was elevated, the interaction between $[Rh_{10}Se]$ and TiO_2 surface monotonously increased on the basis of the increase of r_{Rh-Rh} and $N_{Rh-O_{(s)}}$, and the decrease of N_{Rh-Rh} (Table 4). On the other hand, the interaction between Se and $[Rh_{10}]$ was strongest when the T_{evac} was 623 K on the basis of r_{Rh-Se}. It is interesting to note that the interaction of Se with the $O_{(s)}$ atom of TiO_2 was suggested when the T_{evac} was above 623 K (Table 3).

Proposed model structures of $[Rh_{10}Se]$ on TiO_2 surface are illustrated in Fig. 5. As the obtained $N_{Rh-O_{(s)}}$ values were relatively large (1.2–1.7), the exposure of surface-oxygen-rich $TiO_2(110)$ face was assumed (21). The $[Rh_n]$ ($n = 3$–5) face was assumed to be in parallel to the TiO_2 face. As suggested above, the $[Rh_{10}Se]$ should interact with TiO_2 surface through the $[Rh_3]$ face when the T_{evac} was 523 K (Fig. 5a). If each of the three interface Rh atoms bonded to four O atoms, the $N_{Rh-O_{(s)}}$ should be 1.2 in average (the cluster has 10 Rh atoms), equal to the value obtained by EXAFS. If the $r_{Rh-O_{(s)}}$ was fixed to 2.10 Å (Table 4) in average, the $Se-O_{(s)}$ distance was calculated 2.62 Å. This longer coordination compared to Se–Rh (2.44 Å) may not be detected by curve fitting analysis in Table 3.

Figure 5b illustrates the structure of $[Rh_{10}Se]/TiO_2$ heated at 623 K. In a similar procedure to a, the model was constructed. It reproduced well the EXAFS data. The metrical parameters of model b was r_{Rh-Rh} of 2.72 Å, r_{Rh-Se} of 2.41 Å, $r_{Rh-O_{(s)}}$ of 2.09 Å, $N_{Rh-O_{(s)}}$ of 1.3, and $r_{Se-O_{(s)}}$ of 1.97 Å, compared to the values in Tables 3 and 4 (2.72, 2.41, 2.09, 1.5, and 1.97 Å, respectively). The interface model of Fig. 5c corresponds to the $[Rh_{10}Se]/TiO_2$ heated at 813 K. The model c was with r_{Rh-Rh} of 2.75 Å, r_{Rh-Se} of 2.43 Å, $r_{Rh-O_{(s)}}$ of 2.14 Å, $N_{Rh-O_{(s)}}$ of 1.4, and $r_{Se-O_{(s)}}$ of 1.98 Å in good coincidence with values in Tables 3 and 4 (2.75, 2.42–2.43, 2.13, 1.7, 1.98 Å, respectively). The interface model of $[Rh_{10}Se]/SiO_2$ with $r_{Se-O_{(s)}}$ of 1.95 Å (Table 3) could be constructed on the relatively stable $SiO_2(111)$ face (22).

Electronic State of [$Rh_{10}Se$] on Oxides

The edge positions of Se K-edge and Rh K-edge exhibited shifts within 0.6 eV for Se and within 2.2 eV for Rh. The Se edge position was highest at $T_{evac} = 623$ K, implying largest charge donation to Rh. The Rh K-edge position reached minimum at the temperature, supporting the change donation from Se.

The peak **A** intensity in Rh K-edge spectra (Fig. 3) was in the order (**1**) > $[Rh_{10}Se]/TiO_2$ ($T_{evac} = 523$ K) ≈ $[Rh_{10}Se]/MgO$ > $[Rh_{10}Se]/TiO_2$ ($T_{evac} = 623$ K) > $[Rh_{10}Se]/Al_2O_3$ > $[Rh_{10}Se]/TiO_2$ ($T_{evac} = 813$ K) ≈ $[Rh_{10}Se]/SiO_2$, in accordance with the smallness of r_{Rh-Rh} values except for the $[Rh_{10}Se]/MgO$ (Table 4); the larger the r_{Rh-Rh}, the weaker the peak **A**. The decrease of $1s \rightarrow 4d$ peak intensity as a function of heating temperature was reported at Pd K-edge for Au/Pd bimetallic colloid catalyst (4). In summary, peak **A** and r_{Rh-Rh} demonstrated monotonous change of electronic state of Rh as the increase of T_{evac}.

The $1s \rightarrow np$ transition intensity can be expressed in the dipole approximation (23)

$$I(1s \rightarrow np) \propto |\langle \phi_f | \mathbf{M} | \phi_i \rangle|^2,$$

where **M** is dipole operator and ϕ_i and ϕ_f are the initial and final states, respectively. The peak area varied much in the series of samples of Table 2, suggesting that the transition was $1s \rightarrow 4p$ rather than $1s \rightarrow 5p$. Hence, by a simple approximation on the basis of the peak area in Table 2 (4.2–4.3 for $[Rh_{10}Se]/TiO_2$ and 8.0–8.4 for Se powder and Rh_3Se_8), the valence state of Se was suggested to be ≈−1 for $[Rh_{10}Se]/TiO_2$. The peak area exhibited negligible changes for $[Rh_{10}Se]/TiO_2$ when the heating temperature was varied. Therefore, the Se atom should be always anionic, and the extent of interaction between Se and $[Rh_{10}]$ controlled the electronic state of Rh. The chemical shift of Se for crystal (**1**) and $[Rh_{10}Se]/TiO_2$ was measured by XPS. The Se $3d_{5/2}$ peak was centered at 54.1 and 53.7 eV, respectively, suggesting the valence states of Se of −2–−1.

Reaction Mechanism

The reaction mechanism of ethanol synthesis on $[Rh_{10}Se]/TiO_2$ was studied by *in-situ* FT-IR in $CO_2 + H_2$ (24). The intensity of two peaks at 1614 and 1243 cm^{-1} coupled in the course of reactions. They were assigned to bidentate carbonate species (25). Two peaks were observed in the same region for unimpregnated TiO_2 at 1570 and 1230 cm^{-1} in $CO_2 + H_2$. Two unresolved peaks between the two carbonate peaks were also observed on $[Rh_{10}Se]/TiO_2$. The two peaks may be assigned to acetate species (26). In the case of the reaction of CO_2 compared to of CO, predominant carbonate absorption was too strong to quantitatively measure the acetate absorption. The carbonate species for $[Rh_{10}Se]/TiO_2$ should be affected by $[Rh_{10}Se]$, either being near $[Rh_{10}Se]$ or on Rh of $[Rh_{10}Se]$.

The increase of the peaks at 2965, 2883, 2919, and 2853 cm^{-1} was proportional to the ethanol synthesis rate. They were assigned to CH_3 ν_{as}, ν_s, CH_2 ν_{as}, and ν_s, respectively. The dissociation of C–O bonds of carbon dioxide occurs on Rh and the four peaks rapidly disappeared when the supply of reaction gas ($CO_2 + H_2$) stopped. Therefore, methyl and methylene species should be mainly on Rh. Compared to the cases of [$Rh_{10}Se$] on the other supports (Al_2O_3, SiO_2, and MgO), the stretching peaks of CO at 2174 and 2108 cm^{-1} were weak. The reason why CO(a) was not stabilized on [$Rh_{10}Se$]/TiO_2 may be due to the difference of coordination number around Rh (6.4 ± 0.7) for [$Rh_{10}Se$]/TiO_2 compared to [$Rh_{10}Se$]/Al_2O_3, [$Rh_{10}Se$]/SiO_2, and [$Rh_{10}Se$]/MgO (5.5 ± 0.2). These two wavenumbers were relatively high and suggesting CO on positive Rh sites in accordance with XAFS study.

The CH_3(a) or CH_2(a) on Rh reacted with CO_3(a) or CO_2 to form acetate, followed by the hydrogenation into ethanol on Rh sites. The reaction of $CO + H_2$ was very slow and of entirely different product distribution from the reaction of $CO_2 + H_2$ on [$Rh_{10}Se$]/TiO_2 (1), demonstrating the ethanol synthesis was not via CO in the case of [$Rh_{10}Se$]/TiO_2. The stability of CH_x(ads) on Rh should be pertinent. The "rhodium selenide"-like electronic state poisoned methane formation, and tuned the reaction path to ethanol synthesis by promoting the C–C bond formation of CH_x with carbonyl derivative to form acetate species.

The [$Rh_{10}Se$] clusters on SiO_2, Al_2O_3, and MgO could not catalyze effectively probably because the surface was poisoned by CO(a) due to the very fast process $CO_2 \rightarrow CO(a) + O(a)$ (FT-IR), supported by their lower coordination numbers by EXAFS (5.5 ± 0.2).

CONCLUSIONS

(1) The edge spectra indicated the electronic states of Se and Rh: interstitial Se atom was always anionic while the state of Rh atoms around Se gradually changed.

(2) The EXAFS indicated the minimum r_{Se-Rh} (2.41 Å) for [$Rh_{10}Se$]/TiO_2 when heated at 623 K. The Se-edge and Rh-edge positions supported the strongest interaction between Se and [Rh_{10}] at 623 K.

(3) Ethanol synthesis from CO_2 was observed only when TiO_2 was utilized as support. The higher coordination around active site should be one reason to tune the reaction path to $CH_x(a) + CO_y(a) \rightarrow$ acetate(a) $\rightarrow$ ethanol by suppressing the CO(a) and CH_4 formations.

REFERENCES

1. Kurakata, H., Izumi, Y., and Aika, K., *Chem. Commun.*, 389–390 (1996).
2. Sachtler, W. M. H., *Faraday Discuss. Chem. Soc.* **72**, 7–31 (1981).
3. Sinfelt, J. H., Via, G. H., and Lytle, F. W., *Catal. Rev. Sci. Eng.* **26**, 81–140 (1984).
4. Lee, A. F., Baddeley, C. J., Hardacre, C., Ormerod, R. M., Lambert, R. M., Schmid, G., and West, H., *J. Phys. Chem.* **99**, 6096–6102 (1995).
5. Bradley, J. S., *in* "Clusters and Colloids, From Theory and Applications" (G. Schmid, Ed.), pp. 459–544. VCH, Weinheim, Germany, 1994.
6. Patil, A. N., Andres, R. P., and Otsuka, N., *J. Phys. Chem.* **98**, 9247–9251 (1994).
7. Izumi, Y., and Iwasawa, Y., *CHEMTECH* **24**(July), 20–27 (1994).
8. Izumi, Y., Asakura, K., and Iwasawa, Y., *J. Catal.* **127**, 631–644 (1991).
9. Izumi, Y., Asakura, K., and Iwasawa, Y., *J. Catal.* **132**, 566–570 (1991).
10. Izumi, Y., and Iwasawa, Y., *J. Phys. Chem.* **96**, 10942–10948 (1992).
11. Galli, D., Garlaschelli, L., Ciani, G., Fumagalli, A., Martinengo, S., and Sironi, A., *J. Chem. Soc., Dalton Trans.*, 55–61 (1984).
12. Ciani, G., Garlashelli, L., Sironi, A., and Martinengo, S., *J. Chem. Soc., Chem. Commun.*, 563–565 (1981).
13. Hohnke, D., and Parthe, E., *Z. Kristallogr.* **127**, 164–172 (1968).
14. Pantelouris, A., Kuper, G., Hormes, J., Feldmann, C., and Jansen, M., *J. Am. Chem. Soc.* **117**, 11749–11753 (1995).
15. Bianconi, A., *in* "X-ray absorption: Techniques of EXAFS, SEXAFS, and XANES" (D. C. Koningsberger and R. Prins, Eds.), pp. 573–662. Wiley, New York, 1988.
16. Krause, M. O., and Olivier, J. H., *J. Phys. Chem. Ref. Data* **8**, 329–338 (1979).
17. Yokoyama, T., Hamamatsu, H., and Ohta, T., University of Tokyo, 1994.
18. The Chemical Society of Japan, Ed., *The Chemistry Handbook, Basic Edition;* Maruzen, Tokyo, 1984, p. II-716.
19. Wells, A. F., *Structural Inorganic Chemistry, 3rd Edition;* Oxford University Press, London, 1962, p. 430.
20. Lee, G. v. d., and Ponec, V., *Catal. Rev. Sci. Eng.* **29**, 183–218 (1987).
21. Henrich, V. E., and Kurtz, R. L., *Phys. Rev. B* **23**, 6280–6287 (1981).
22. Sindorf, D. W., and Marciel, G. E., *J. Am. Chem. Soc.* **105**, 1487–1493 (1983).
23. Wong, J., Lytle, F. W., Messmer, R. P., and Maylotte, D. H., *Phys. Rev. B* **30**, 5596–5610 (1984).
24. Izumi, Y., *Platinum Metals Rev.* **41**, 166–170 (1997).
25. Nakamoto, K., *in* "Infrared and Raman Spectra of Inorganic and Coordination Compounds," 3rd ed. Wiley, New York, 1970.
26. Bowker, M., *Catal. Today* **15**, 77–100 (1992).